BRIEF COMMUNICATION
https://doi.org/10.1038/s41592-020-0835-7

nature methods

jYCaMP: an optimized calcium indicator for two-photon imaging at fiber laser wavelengths

Manuel Alexander Mohr[1,2,7], Daniel Bushey[1], Abhi Aggarwal[1,3], Jonathan S. Marvin[1], Jeong Jun Kim[1], Emiliano Jimenez Marquez[1,4], Yajie Liang[1,5], Ronak Patel[1], John J. Macklin[1], Chi-Yu Lee[1], Arthur Tsang[1,5], Getahun Tsegaye[1,5], Allison M. Ahrens[6], Jerry L. Chen[6], Douglas S. Kim[1,5], Allan M. Wong[1,5], Loren L. Looger[1,5], Eric R. Schreiter[1,5] and Kaspar Podgorski[1]✉

Femtosecond lasers at fixed wavelengths above 1,000 nm are powerful, stable and inexpensive, making them promising sources for two-photon microscopy. Biosensors optimized for these wavelengths are needed for both next-generation microscopes and affordable turn-key systems. Here we report jYCaMP1, a yellow variant of the calcium indicator jGCaMP7 that outperforms its parent in mice and flies at excitation wavelengths above 1,000 nm and enables improved two-color calcium imaging with red fluorescent protein-based indicators.

Two-photon (2P) microscopy has become a leading method for in vivo imaging owing to its optical sectioning capabilities and the increased depth-penetration of near-infrared light in scattering tissue[1]. However, the light sources commonly used for 2P imaging—tuneable titanium-sapphire lasers and parametric oscillators—are costly, require frequent expert maintenance and lack the output power needed for operating several microscopes simultaneously or for high-speed imaging methods that use extended focal patterns[2–5].

Promising alternatives to these traditional light sources, such as high-power industrial ytterbium-doped fiber lasers (YbFLs) and modelocked semiconductor lasers, have shown feasibility for in vivo imaging[2–7] and are becoming widely available at costs orders of magnitude lower and/or power outputs orders of magnitude higher than conventional tunable lasers (Supplementary Fig. 1). Since the bulk of a 2P microscope's cost is the laser, these sources promise to make 2P imaging accessible to many more users. However, commercially available lasers of this kind are largely limited to a fixed wavelength of approximately 1,030–1,080 nm, which poorly excites most green fluorescent protein (GFP)-based biosensors such as the GCaMPs, the best-in-class genetically encoded fluorescent Ca^{2+} indicators (GECIs) (Fig. 1b). To take advantage of inexpensive and powerful industrial lasers, high-performance biosensors that excite at wavelengths above 1,000 nm are needed. 2P imaging of GECIs has become widespread for monitoring neuronal activity and is vital to modern neuroscience[1]. We therefore set out to identify spectral variants of the recently developed jGCaMP7 family of GECIs[8] with improved 2P excitation at fiber laser wavelengths.

Mutations can convert GFPs to yellow fluorescent proteins that are well-excited at 1,030 nm. Substitution of T115 (position 203 in GFP) with an aromatic amino acid allows this residue to form a π-stacking interaction with the phenolic ring of the GYG-chromophore (compared to the green TYG-chromophore) resulting in a shift toward longer wavelengths[9]. To redshift jGCaMP7, we first introduced mutations that convert GFP into mVenus[10] ('Venus-GCaMP'; jGCaMP7s + M65T, V115Y, K118V, F203L, T222G, V225L, S229A, I250A). Unfortunately, Venus-GCaMP did not exhibit the anticipated spectral shift, retaining excitation and emission spectra similar to its parent GCaMP (Supplementary Fig. 2). To find a truly yellow-fluorescent GCaMP variant, we randomly mutated Venus-GCaMP, and used fluorescence emission ratiometry to screen for spectral shift in bacterial colonies. We found a single amino acid mutation S117P (205 in GFP), close to T115, that produced a pronounced redshift. The resulting variant maintained sensor properties similar to those of the parent GCaMP while exhibiting 19 and 36 nm spectral shift in its one-photon and 2P excitation spectrum, respectively (Fig. 1b and Supplementary Table 1). Similarly, jGCaMP7 variants containing yellow fluorescent protein, YPET and citrine mutations failed to produce yellow emission spectra but were rescued by additional introduction of the S117P mutation (data not shown). In GCaMP, the closed barrel structure of circularly permuted GFP is opened within β-strand 7 to accommodate the calcium-sensing domains. Residues 115 and 117 lie on β-strand 10 of GFP, structurally adjacent to β-strand 7, and their position might be affected by the GCaMP permutation in a way that prevents the crucial π-stacking interaction (Fig. 1a). The substitution S117P might then reorient position 115 to rescue the π-stacking and yield the observed yellow fluorescence.

Among jGCaMP7 variants, jGCaMP7b and jGCaMP7s containing the mVenus and S117P mutations (M65T, V115Y, S117P, K118V, F203L, T222G, V225L, S229A, I250A) exhibited the largest fluorescence responses to field stimulation in neuron cultures (Fig. 1c and Supplementary Fig. 3). These variants, called 'jYCaMP1' and 'jYCaMP1s', respectively, have slightly higher Ca^{2+} affinity than their jGCaMP7b and 7s parents (Supplementary Fig. 4 and Supplementary Table 1) and show responses similar to those of GCaMP6s at its one-photon excitation optimum (Fig. 1c). Under redshifted illumination, they showed significantly larger $\Delta F/F$ responses than GCaMP6s for one or three action potentials (four- and twofold larger, respectively, for both indicators, Supplementary Fig. 3). jYCaMP1 and jYCaMP1s also had 2.7-fold higher

[1]Janelia Research Campus, Howard Hughes Medical Institute, Ashburn, VA, USA. [2]Department of Biosystems Science and Engineering, Eidgenössische Technische Hochschule Zurich, Basel, Switzerland. [3]Department of Chemistry, University of Alberta, Edmonton, Alberta, Canada. [4]Universidad Nacional Autonoma de Mexico, Mexico, Mexico. [5]GENIE Project, Janelia Research Campus, Howard Hughes Medical Institute, Ashburn, VA, USA. [6]Department of Biology, Boston University, Boston, MA, USA. [7]Present address: Department of Biology, Stanford University, Stanford, CA, USA. ✉e-mail: podgorskik@janelia.hhmi.org

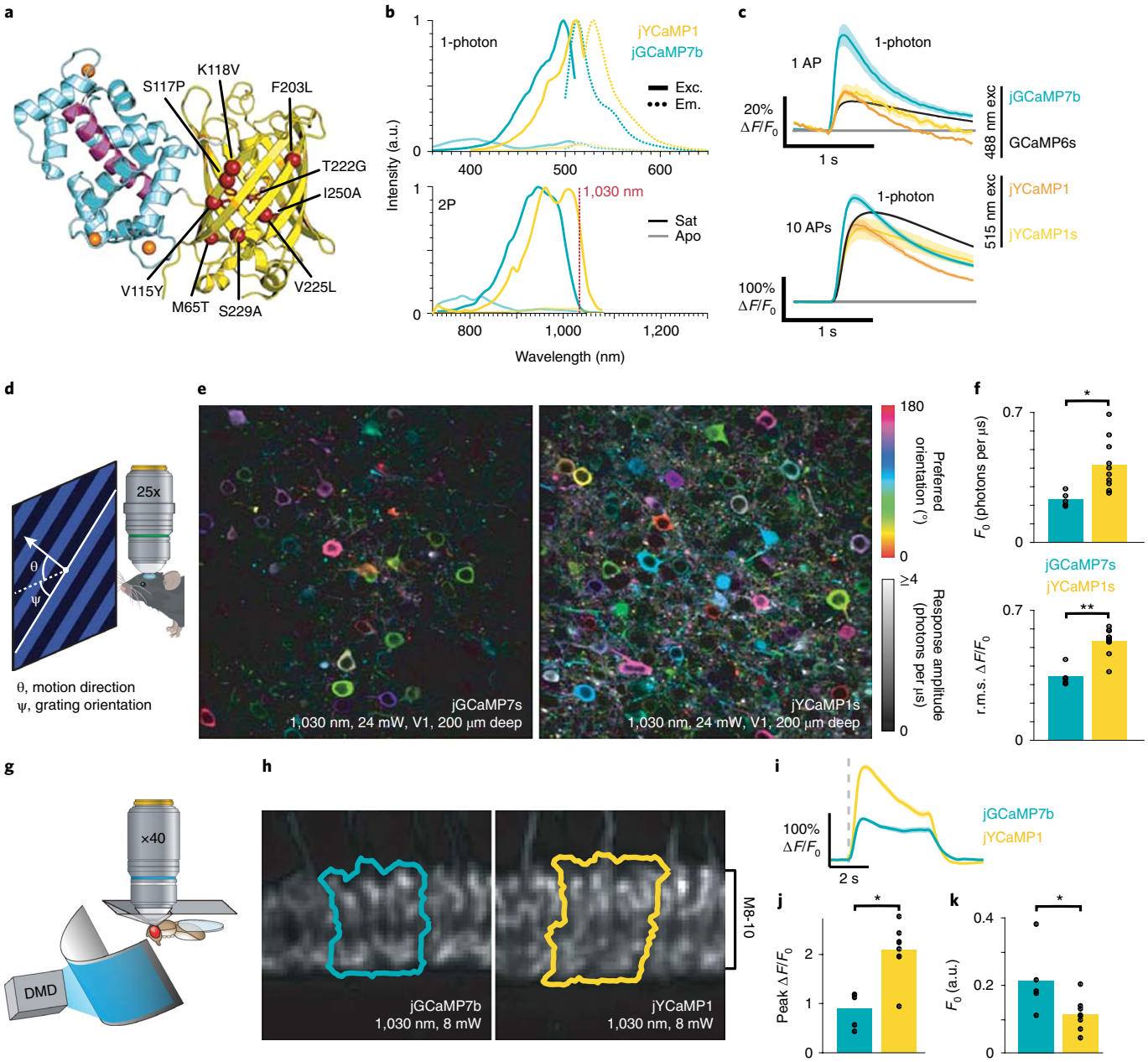

Fig. 1 | jYCaMP1 is a redshifted variant of jGCaMP7 capable of detecting single action potentials. a, Schematic of jYCaMP1 mutations (red spheres) overlaid on the GCaMP structure (PDB ID 3EVR, ref. [11]). **b**, Normalized one-photon excitation (solid lines) and emission (dotted lines) spectra (top) and 2P action cross-sections (bottom) in the presence and absence of calcium, for jYCaMP1 and jGCaMP7b. **c**, Responses in rat primary hippocampal cultures to one and ten action potentials for indicators at their respective excitation optima. GCaMP6s and jGCaMP7b data, acquired on the same apparatus as jYCaMP data, are reprinted from ref. [8]. Shading denotes s.e.m. N (no. of wells) = 104 jGCaMP7b, 682 GCaMP6s, 11 jYCaMP1 and ten jYCaMP1s. **d**, Anesthetized mice were shown visual stimuli while recording activity in layer 2/3 of the visual cortex. **e**, Orientation tuning maps in examples of jGCaMP7s and jYCaMP1s expressing FOV. Hue denotes preferred orientation and brightness denotes response amplitude. Some pixels are saturated. Similar results were obtained for $N = 5$ (jGCaMP7s) and $N = 10$ (jYCaMP1s) FOV. **f**, Mean baseline intensity of responsive ($\Delta F/F > 1$) pixels (top) and mean $\Delta F/F$ of bright ($F_0 > 0.5$) pixels (bottom), for $N = 5$ (jGCaMP7s) and $N = 10$ (jYCaMP1s) FOV. Dots denote individual FOV, bars indicate mean. $P = 0.01$ (F_0), $P = 0.0001$, (r.m.s. $\Delta F/F$), two-sided two-sample t-tests. **g**, Flies were head fixed to a pyramidal plate with the cuticle above the Mi1 neurons removed for imaging, and presented full-field visual stimuli. **h**, Sample regions of interest, typical of $N = 8$ (jYCaMP1), $N = 5$ (jGCaMP7b) flies, drawn around the columns in layers 8–10 of the medulla that showed the largest increase in intensity to the stimulation. **i**, $\Delta F/F$ responses in Mi1 neurons expressing jYCaMP1 and jGCaMP7b. Gray dashed line presents stimulus onset (lights on). **j**, Maximum $\Delta F/F$ reached after stimulation. $P = 1 \times 10^{-4}$, two-sided two-sample t-test. **k**, Baseline fluorescence before stimulation. $P = 0.033$, two-sided two-sample t-test. **j**,**k**, $N = 8$ (jYCaMP1), $N = 5$ (jGCaMP7b) flies. Dots denote individual FOV, bars indicate mean.

molecular brightness than jGCaMP7b when excited at 1,030 nm (Supplementary Fig. 5) and differed substantially from each other only in response kinetics. These properties suggested that jYCaMPs might outperform the best green GECIs in vivo when imaged using 2P excitation at or beyond 1,030 nm, so we further characterized them in mice and flies.

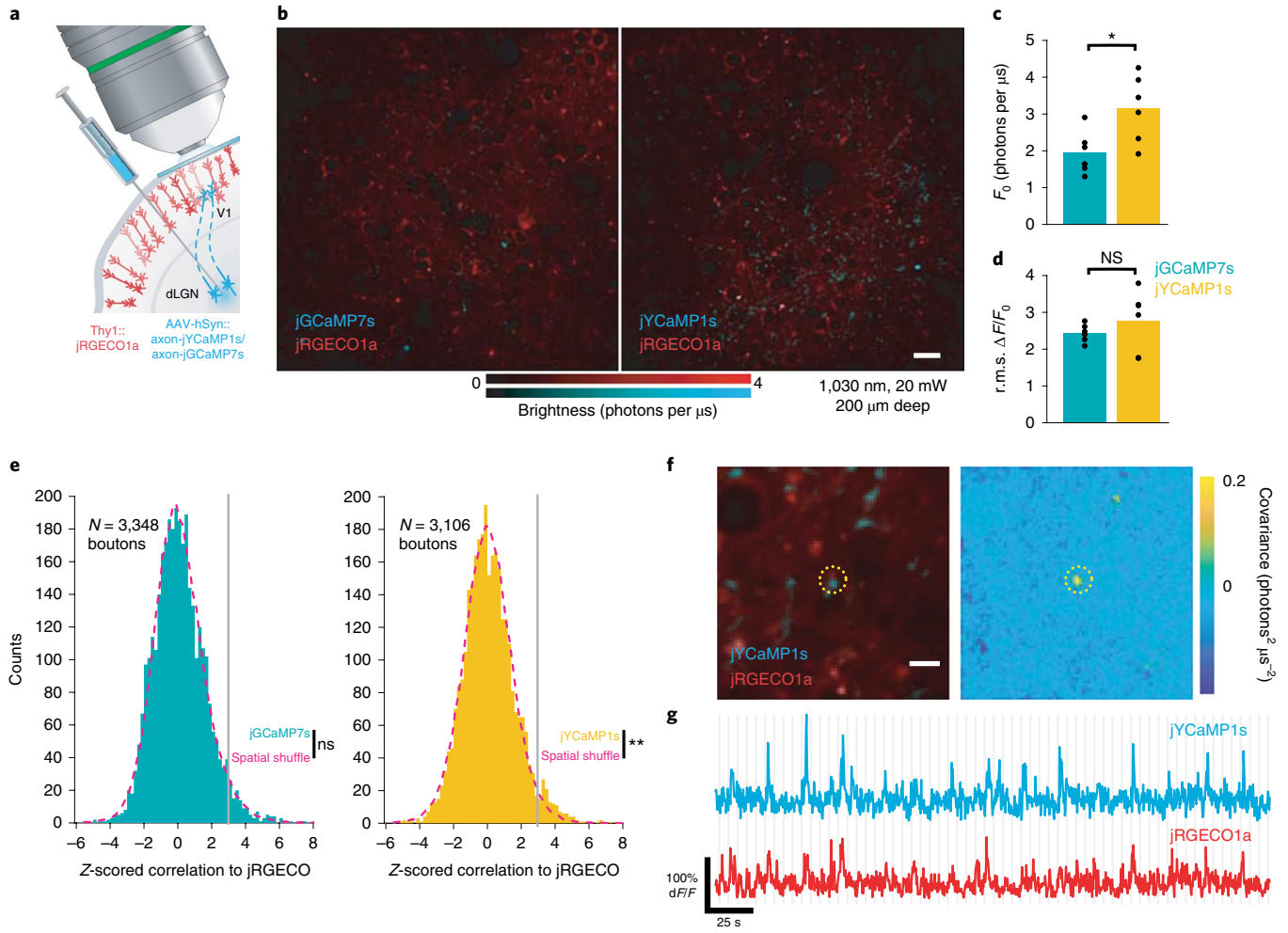

Fig. 2 | jYCaMP1 enables brighter two-color calcium imaging together with red GECIs, improving correlation analysis of overlapping compartments. **a**, Schematic of two-color cortical labeling. Virus encoding axon-targeted jGCaMP7s or jYCaMP1s was injected into the dLGN of thalamus in transgenic *Thy1:jRGECO1a* mice, and visually evoked activity recorded in cortex. **b**, Example FOV expressing jGCaMP7s and jYCaMP1s. Similar results were obtained for $N=6$ FOV each sensor. Scale bar, 20 µm. **c**,**d**, Mean brightness (**c**) and r.m.s. $\Delta F/F$ response (**d**) of putative boutons ($N=6$ FOV, 3,106 boutons jYCaMP1s, $N=6$ FOV, 3,348 boutons, jGCaMP7s). *$P=0.02$, two-tail, two-sample *t*-test. Markers denote individual FOV. **e**, Distribution of *Z*-scored correlations (Pearson's *r*) between unmixed jRGECO and jGCaMP7s or jYCaMP1s responses at individual putative boutons, and corresponding null distributions obtained by shuffling bouton locations. $P=0.484$ (jGCaMP7s) $P<0.004$ (jYCaMP1s) Kolmogorov–Smirnov test. $N=3,348$ boutons (jGCaMP7s), $N=3,106$ boutons (jYCaMP1s). **f**,**g**, An example jYCaMP1s-labeled putative bouton highly correlated to dendritic jRGECO response. Similar correlated sites were found in five of six FOV. **f**, Left, the average image of each channel and right, pixelwise covariance of response amplitudes across channels. Dotted circle denotes the same area in both images. Scale bar, 5 µm. **g**, jYCaMP and jRGECO recordings from the bouton site. Gray lines denote stimulus onsets (**f**,**g**).

In mice, we imaged jYCaMP1s activity in layer 2/3 of primary visual cortex (V1) while displaying moving grating visual stimuli to the mouse's contralateral eye. Compared to jGCaMP7s, recordings from jYCaMP1s-labeled neurons were 1.8-fold as bright ($P=0.01$, two-sample *t*-test) and showed 1.6-fold $\Delta F/F$ ($P=1\times10^{-4}$, two-sample *t*-test) under 1,030 nm illumination (jYCaMP1s, $n=10$ fields of view (FOV) in four independent animals; jGCaMP7s, $n=5$ FOV, in three independent animals, Fig. 1d–f and Supplementary Fig. 6). jYCaMP's brightness and sensitivity at 1,030 nm enabled simultaneous high-speed imaging of multiple dendritic branches using YbFL-based 2P tomography (Supplementary Fig. 7), and multi-area imaging using 1,040 nm excitation (Supplementary Fig. 8).

In flies, we measured jYCaMP1 activity in Mi1 or Tm3 neurons in the medulla of the optic lobe while presenting whole-field flashing light stimuli (Fig. 1g,k and Supplementary Fig. 9). Light increments produce stereotyped calcium transients in both neuron types[12–14]. In Mi1 (medulla layers 8–10), jYCaMP1 was 0.53-fold as bright as its parent jGCaMP7b at baseline ($P=0.033$, two-sample *t*-test; Fig. 1k) and showed 2.3-fold $\Delta F/F$ ($P=1\times10^{-4}$, two-sample *t*-test, Fig. 1j) under 1,030 nm excitation (jYCaMP1, $n=8$ flies; jGCaMP7b, $n=5$ flies). In Tm3 (lobula plate layer 1), jYCaMP1 was 0.62-fold as bright as jGCaMP7b at baseline ($P=0.011$, two-sample *t*-test) and showed 2.3-fold $\Delta F/F$ responses ($P=5\times10^{-3}$, two sample *t*-test; jYCaMP1, $n=6$ flies and jGCaMP7b = 5 flies, Supplementary Fig. 9).

The ability to record in distinct spectral channels is an important strength of fluorescence imaging. For example, targeting spectrally resolved sensors to different compartments enables simultaneous recording from compartments that are too close together to resolve spatially[15], such as pre- and postsynapses. The 2P excitation spectrum of GCaMP overlaps poorly with state-of-the-art red GECIs such as jRGECO1a, complicating simultaneous two-color Ca^{2+}-imaging[16]. The shifted excitation spectrum of jYCaMP1 greatly improves this overlap while retaining well-separated emission with red sensors, making these GECIs an ideal combination for

simultaneous dual-color 2P Ca^{2+}-imaging with a single excitation laser. To test the capabilities of jYCaMP for two-color imaging with red GECIs, we performed simultaneous Ca^{2+}-imaging of thalamocortical projections labeled with axon-targeted[17] jYCaMP1s and cortical dendrites labeled with jRGECO1a (Fig. 2a,b see Methods).

Under 1,030 nm excitation, jYCaMP1s enabled us to routinely record axonal responses with 20 mW of excitation power (Fig. 2b), showing 1.6-fold baseline brightness and similar response amplitudes to jGCaMP7s (jYCaMP1s, six FOV, five mice, 3,106 boutons and jGCaMP7s, six FOV, four mice, 3,348 boutons; see Fig. 2c,d). Simultaneous 1,030 nm excitation of jYCaMP1s and jRGECO1a enabled recording of distinct Ca^{2+} dynamics in spatially overlapping axonal and dendritic compartments, which has been used to identify putative synapses[16,18,19]. We compared jGCaMP7s to jYCaMP1s for such detection of coactive axons and dendrites, based on trial-to-trial correlations to dendritic jRGECO responses at putative boutons. Using jGCaMP7s, at false positive rate of 1%, 1.01% of boutons showed significant correlations and the observed distribution did not vary significantly from the null ($P=0.484$, two-sample Kolmogorov–Smirnov test). Using jYCaMP1s, at false positive rate of 1%, 2.22% of boutons showed significant correlations, and the distribution differed significantly from the null ($P=0.004$, two-sample Kolmogorov–Smirnov test, Fig. 2e). Significantly correlated sites contained bright structures in both channels and highly coordinated dynamics (Fig. 2f,g). These results demonstrate that jYCaMP's improved coexcitation with red fluorescent proteins facilitates challenging two-color experiments, which previously required high excitation powers[16,18,19] that can damage neurites[20].

In summary, we generated jYCaMP1, a variant of jGCaMP7 with a redshifted excitation spectrum. This yellow-fluorescent GECI inherits the high Ca^{2+} affinity and excellent in vitro and in vivo performance characteristics of its optimized parent protein. Its redshifted excitation spectrum is compatible with inexpensive 1,030 and 1,040 nm lasers, enabling high-performance in vivo calcium imaging, high-speed methods requiring large pulse energies, and efficient single-laser two-color imaging alongside red GECIs. Other potential applications include compact optical systems incorporating miniaturized low-cost lasers, or multiplexing many microscopes using a single high-power source. In combination with other labels[2,5] and functional indicators[16] excitable at these wavelengths, jYCaMP1 will enable a rich variety of experiments using only inexpensive fixed-wavelength lasers without losses in signal quality.

Online content

Any methods, additional references, Nature Research reporting summaries, source data, extended data, supplementary information, acknowledgements, peer review information; details of author contributions and competing interests; and statements of data and code availability are available at https://doi.org/10.1038/s41592-020-0835-7.

Received: 23 October 2019; Accepted: 14 April 2020;
Published online: 25 May 2020

References

1. Grienberger, C. & Konnerth, A. Imaging calcium in neurons. *Neuron* **73**, 862–885 (2012).
2. Voigt, F. F. et al. Multiphoton in vivo imaging with a femtosecond semiconductor disk laser. *Biomed. Opt. Express* **8**, 3213 (2017).
3. Kazemipour, A. et al. Kilohertz frame-rate two-photon tomography. *Nat. Methods* **16**, 778–786 (2019).
4. Wu, J. et al. Kilohertz two-photon fluorescence microscopy imaging of neural activity in vivo. *Nat. Methods* **17**, 287–290 (2020).
5. Perillo, E. P. et al. Deep in vivo two-photon microscopy with a low cost custom built mode-locked 1060 nm fiber laser. *Biomed. Opt. Express* **7**, 324 (2016).
6. Kim, D. U. et al. Two-photon microscopy using an $Yb^{(3+)}$-doped fiber laser with variable pulse widths. *Opt. Express* **20**, 12341 (2012).
7. Tilma, B. W. et al. Recent advances in ultrafast semiconductor disk lasers. *Light Sci. Appl.* **4**, e310–e310 (2015).
8. Dana, H. et al. High-performance calcium sensors for imaging activity in neuronal populations and microcompartments. *Nat. Methods* **16**, 649–657 (2019).
9. Ormö, M. et al. Deletions of the *Aequorea victoria* green fluorescent protein define the minimal domain required for fluorescence. *Science* **273**, 1392–1395 (1996).
10. Nagai, T. et al. A variant of yellow fluorescent protein with fast and efficient maturation for cell-biological applications. *Nat. Biotechnol.* **20**, 87–90 (2002).
11. Wang, Q., Shui, B., Kotlikoff, M. I. & Sondermann, H. Structural basis for calcium sensing by GCaMP2. *Structure* **16**, 1817–1827 (2008).
12. Behnia, R., Clark, D. A., Carter, A. G., Clandinin, T. R. & Desplan, C. Processing properties of ON and OFF pathways for *Drosophila* motion detection. *Nature* **5212**, 427–430 (2014).
13. Strother, J. A. et al. The emergence of directional selectivity in the visual motion pathway of *Drosophila*. *Neuron* **94**, 168–182.e10 (2017).
14. Strother, J. A., Nern, A. & Reiser, M. B. Direct observation of ON and OFF pathways in the *Drosophila* visual system. *Curr. Biol.* **24**, 976–983 (2014).
15. Valm, A. M. et al. Applying systems-level spectral imaging and analysis to reveal the organelle interactome. *Nature* **546**, 162–167 (2017).
16. Dana, H. et al. Sensitive red protein calcium indicators for imaging neural activity. *Elife* **5**, e12727 (2016).
17. Broussard, G. J. et al. In vivo measurement of afferent activity with axon-specific calcium imaging. *Nat. Neurosci.* **21**, 1272–1280 (2018).
18. Inoue, M. et al. Rational engineering of XCaMPs, a multicolor GECI Suite for in vivo imaging of complex brain circuit dynamics. *Cell* **177**, 1346–1360.e24 (2019).
19. Sun, Y. et al. Neural signatures of dynamic stimulus selection in *Drosophila*. *Nat. Neurosci.* **20**, 1104–1113 (2017).
20. Podgorski, K. & Ranganathan, G. Brain heating induced by near-infrared lasers during multiphoton microscopy. *J. Neurophysiol.* **116**, 1012–1023 (2016).

Methods

Animal care and use statement. All surgical and experimental procedures were in accordance with protocols approved by the Howard Hughes Medical Institute (HHMI) Janelia Research Campus Institutional Animal Care and Use Committee and Institutional Biosafety Committee. This research has complied with all relevant ethical regulations.

Molecular biology. Bacterial expression plasmids for jYCaMP1 and jYCaMP1s were created by replacing the fluorescent protein portion in pRSET-jGCaMP7 (gift from D. Kim) through restriction digest (SacI and AflII) and isothermal assembly of synthesized gene fragments (GBlocks). Randomized libraries were created using isothermal assembly of a Mutazyme (Agilent) PCR according to the manufacturer's suggestions. Depletion of individual mutations was performed using a QuikChange Site-Directed Mutagenesis Kit (Agilent Technologies Inc.) according to the manufacturer's suggestions. Plasmid sequences were confirmed via Sanger sequencing.

Bacterial colony screen. Bacterial colonies on agar plates were screened for bathochromic fluorescence shift on a modified fluorescence stereo microscope (Leica M165 FC, Leica Microsystems) with a coupled mercury metal halide light source (Leica EL6000, Leica Microsystems). Illumination and emitted light were initially split by the microscope dichroic (GFP-LP, Leica) followed by a custom filter cube (ET510/20m, ET537/29m, T525LPXR; Chroma) to produce two narrow-band channels for emission ratiometry. These images were detected by CMOS cameras (Blackfly S Mono 5.0 MP, GigE Vision). A custom MATLAB script displayed the two channels overlaid in false color at a user defined ratio, allowing the user to rapidly visualize subtle spectral variations. Colonies that appeared redshifted were picked for further analysis.

Protein expression and in vitro analysis. Recombinant sensor proteins were expressed in autoinduction medium according to known protocols[21]. Ca^{2+}-saturated and Ca^{2+}-free measurements were performed in 39 µM free Ca^{2+} (+Ca^{2+}) buffer (30 mM MOPS, 10 mM CaEGTA in 100 mM KCl, pH 7.2) or 0 µM free Ca^{2+} (-Ca^{2+}) buffer (30 mM MOPS, 10 mM EGTA in 100 mM KCl, pH 7.2), respectively.

One-photon photophysical measurements. Absorbance measurements were performed using a ultraviolet (UV)-visible spectrum spectrometer (Lambda 35, PerkinElmer). Quantum yield measurements were performed using an integration sphere spectrometer (Quantaurus, Hamamatsu) for proteins in +Ca buffer. Extinction coefficients were determined using alkali denaturation method using extinction coefficient of denatured GFP as a reference (44,000 $M^{-1}cm^{-1}$ at 447 nm).

Ca^{2+}-titrations as well as measurements of kinetic parameters were performed as previously described[16,22,23].

2P measurements. The 2P excitation spectra were obtained as previously described[24]. Protein solutions of 2–4 µM concentration in +Ca^{2+} or -Ca^{2+}- buffer were prepared and measured using an inverted microscope (IX81, Olympus) equipped with a ×60, 1.2 numerical aperture (NA) water-immersion objective (Olympus). 2P excitation was obtained using an 80 MHz Ti::sapphire laser (Chameleon Ultra II, Coherent) for spectra from 710 to 1,080 nm. Fluorescence collected by the objective was passed through a shortpass filter (720SP, Semrock) and a bandpass filter (550BP88, Semrock), and detected by a fiber-coupled Avalanche Photodiode (SPCM_AQRH-14, PerkinElmer). The obtained 2P excitation spectra was normalized for 1 µM concentration.

Fluorescence correlation spectroscopy was used to obtain the 2P molecular brightness of the proteins. The peak molecular brightness was defined by the rate of fluorescence obtained per total number of emitting molecules[25]. The 50–100 nM protein solutions were prepared in +Ca^{2+} buffer and excited with 1,030 nm wavelength at various power ranging from 2–30 mW for 200 s. The obtained fluorescence at was collected by an Avalanche Photodiode and fed to an autocorrelator (Flex03LQ, Correlator.com). The obtained autocorrelation curve was fit on a diffusion model through an inbuilt MATLAB function[25] to determine the number of molecules N present in the focal volume. The 2P molecular brightness at each laser power was calculated as the average rate of fluorescence F per emitting molecule N, defined in kilocounts per second per molecule.

Characterization in neuronal culture. E18 rat cortical neurons nucleofected with pAAV-Synapsin1-jYCaMP1 (or jGCaMP, respectively) variants were stimulated and imaged at 18 d in vitro in the presence of synaptic blockers as described previously[26]. The 35 Hz imaging was performed using a ×10 0.4 NA objective, a X-cite exacte mercury lamp and an ex500/30, T515LP, em535/30 filter cube at 3.5 mW at the sample plane. Cell bodies were segmented, the background subtracted and the relevant parameters extracted as described previously[26].

Mouse surgical procedures. All vertebrate procedures were in accordance with protocols approved by the HHMI Janelia Research Campus Institutional Animal Care and Use Committee (IACUC 17–155). Emx1-Cre (B6.129S2-Emx1$^{tm1(cre)Krj}$/J, Jackson Laboratories) and GP8.50 (Thy1::jRGECO1a, provided by the GENIE project, HHMI Janelia Research Campus) mice (either gender) were intracranially injected with AAV2/1-*Synapsin1*-FLEX-jYCaMP1 or AAV2/1-*Synapsin1*-FLEX-jGCaMP7s, respectively, and AAV2/1-*Synapsin 1*-FLEX-axon-jYCaMP1s or AAV2/1-*Synapsin1*-FLEX-axon-jGCaMP7s, respectively, together with AAV2/1-*Synapsin1*-Cre through a craniotomy and a 4 mm cranial window was placed over the visual cortex. Mice were anesthetized using isoflurane in oxygen (3–4% for induction, 1.5–2% for maintenance), placed on a 37 °C heated pad, administered Buprenorphine HCl (0.1 mg kg^{-1}) and ketoprofen (5 mg kg^{-1}). The skin covering the skull was removed, the sutures of the frontal and parietal bones were sealed with a thin layer of cyanoacrylate glue and a titanium headbar was glued over the left visual cortex. A ~4.5 mm craniotomy (centered 3.5 mm lateral and 0.5 mm rostral of lambda) was performed leaving the dura intact. Glass capillaries (Drummond Scientific, 3-000-203-G/X) pulled and beveled to 30° angle, 20 µm outer diameter loaded into a precision injector (Drummond Scientific, Nanoject III) were used for injections. For experiments comparing axon-jGCaMP7s and axon-jYCaMP1s, mice of the same gender from the same litter were injected on the same day.

For V1 injections, the virus was diluted to 2×10^{12} gc ml^{-1} and slowly injected (1 nl s^{-1}) in 6–8 different injection sites around L2.7 mm; 0.2 mm anterior to lambda; 300 µm deep and 30 nl per site.

For thalamic injections the sensor encoding virus was diluted to 2×10^{12} gc ml^{-1}, mixed 1:1 with 2×10^{9} GC ml^{-1} AAV2/1-*Synapsin1*-Cre and the mix slowly injected (1 nl s^{-1}) in the dLGN (~2.1 mm posterior to bregma, ~2.3 mm left of midline) at two depths (0.5 mm apart, centered at ~2.55 mm deep) and 80 nl per site. Adjusted coordinates for each litter were established via test injections of fluorescent beads in sex-matched littermates, followed by sectioning and microscopic analysis.

The craniotomy was then covered with a 4 mm round no. 1.5 cover glass that was fixed to the skull with cyanoacrylate glue. The animals were imaged 3–6 weeks after surgery. For experiments comparing jGCaMP7b and jYCaMP1s, mice were imaged using the same excitation laser powers, broadband filter sets, and detectors settings.

In vivo imaging of visual responses in mouse visual cortex. Roughly 2–4 weeks after viral injection, the mice were anesthetized using isoflurane, head fixed and restrained inside a custom-built heated holder to restrict movement and maintain a body temperature of 37 °C. A vertically oriented screen (ASUS PA248Q LCD monitor, 1,920 × 1,200 pixels), with a high-extinction 500 nm shortpass filter (Wratten 47B-type) was placed 17 cm from the right eye of the mouse, centered at approximately 65° of azimuth and −10° of elevation. Moving bar stimuli were generated in MATLAB using the Psychtoolbox (20 repetitions of 0.153 cycles per cm, 1 cycle per second, 22° of visual field per second, 2 s duration) in eight equally spaced directions spaced by equal time periods of mean luminance and were shown to the animal synchronized with the acquisition.

Imaging was performed on a home-built 2P microscope equipped with an Insight DS Dual 120 femtosecond-pulse laser (Spectra-Physics) at 1,030 nm, a XLPLN25XWMP2 ×25 1.05 NA water-immersion lens (Olympus) and two silicon photomultiplier detectors (Hamamatsu, custom part, see ref. [3] for details) with 540/80 and 650/90 bandpass filters. The 512 × 512 images were acquired at 3.41 Hz and 21–24 mW postobjective power using ScanImage software (Vidrio Technologies).

Raster recordings were aligned using custom MATLAB scripts as described previously[3]. For Figs. 1e,f and 2c,d, analyses were performed pixelwise. F_0 was calculated as the mean pixel brightness during the four frames before each stimulus onset. Eight-point tuning curves were calculated as the mean pixel brightness during the stimulus period, minus F_0. The preferred orientation (hues in Figs. 1e and 2f) was calculated by vector summation of the tuning curve over the four stimulus orientations (that is, 0, 90, 180, 270, 0, 90, 180 and 270° for the eight stimulus directions). The response amplitude is the two-norm of the eight-point tuning curve, and r.m.s. $\Delta F/F_0$ (Figs. 1f and 2c) is the response amplitude divided by F_0. We plotted the mean F_0 for pixels with response amplitude of >1 photon per µs (jGCaMP7s, 6.9×10^5 responsive pixels, five FOV, three mice. jYCaMP1, 1.5×10^6 responsive pixels, ten FOV, four mice) and the r.m.s. dF/F for pixels with $F_0 > 1$ photon per µs (jGCaMP7s, 5.0×10^5 bright pixels; jYCaMP1, 1.0×10^6 bright pixels).

Scanned line angular projection (SLAP) imaging[3] was performed in the V1 of a Chrna2-OE25/C57Bl6J heterozygous mouse (a line that expresses Cre recombinase in a sparse subset of L5 pyramidal neurons) injected with AAV2/1.*hSynapsin1*. FLEX.jYCaMP1s. Imaging was performed at 500 Hz using a 1,030 nm YbFL (BlueCut, Menlo Systems) with the abovementioned visual stimuli. Segments of interest (Supplementary Fig. 7) were manually drawn, and remaining regions of the three-dimensional reference image were segmented automatically using the SLAP software package (www.github.com/KasparP/SLAP). Reconstructions were performed using the SLAP software package using a time constant of 20 ms, baseline of 0.8 and default parameters otherwise.

Dual-color in vivo Ca^{2+}-imaging in the mouse cortex. Dual-color cortical imaging experiments (Fig. 2) were performed using the same hardware, stimuli and microscope settings as one-color cortical imaging. We used GP8.50

Thy1:jRGECO1a transgenic mice, in which approximately 50% of layer 2/3 and layer five neurons are labeled. All recordings were performed 200 µm below the surface of the pia using 20 mW of postobjective laser power. Automated detection of boutons was used to quantify brightness and responsiveness of axon-targeted jGCaMP7s and jYCaMP1.

Putative boutons were detected as local maxima in the green channel average intensity image that were brighter than a quarter of the 95th percentile of the image intensity, after smoothing with a sigma = 0.5 µm Gaussian kernel. We plotted the mean F_0 and r.m.s. $\Delta F/F_0$ treating FOV as the unit of variation (GCaMP, six FOV; four mice, 3,348 boutons; jYCaMP, six FOV, five mice, 3,106 boutons).

The red and green/yellow emission bands of the fluorophores we used are well separated, and can be collected with only mild tradeoffs between collection efficiency and crosstalk in their tails. To remove residual crosstalk, red and green channels were linearly unmixed before analysis and display, using least squares unmixing (mixing proportions for our filters and detector sensitivities: jGCaMP/RGECO 0.022 green to red, 0.11 red to green; jYCaMP/RGECO 0.08 green to red, 0.11 red to green). To design effective analyses of correlations between axonal and dendritic compartments (Fig. 2e–g), we performed simulations that assessed effects of bleed through and unmixing on measured correlations, and validated the generation of null distributions for statistical comparisons. These simulations showed that least squares spectral unmixing of Poisson-distributed measurements results in negative bias in computed sample correlations. We found that maximum likelihood unmixing of Poisson-distributed measurements results in positive bias, and did not use it in our studies. To compensate for bias and better normalize comparisons across FOV and imaging conditions, sample correlations for each FOV were *Z* scored according to the null distribution computed for that FOV. *Z* scores were computed by subtracting the median of the sample distribution and dividing by the standard deviation of the spatially shuffled null distribution. The spatially shuffled null distribution was also *Z* scored. Detection rates reported were computed by pooling the *Z*-scored correlations across FOV, and comparing to the pooled null distribution samples. Spatial shuffling consisted of randomly reassigning the bouton identities, but not the timeseries, for one channel (after unmixing) before computing the correlations between the channels. We validated that the computed and Z-scored null distributions accurately represent the *Z*-scored sample correlations for uncorrelated latents across a wide range of mean photon rates (1–1,000 detected photons), mixtures of photon rates across boutons and channels and a variety of activity distributions (Gaussian, binary, Poisson, spike and slab), and are robust to errors in unmixing coefficients of up to 50%. MATLAB code that performs these simulations is available at www.github.com/KasparP/TwoColorUnmixing.

Detection rates at 1% false positives reported were computed as the fraction of pooled correlations that exceeded the 99th percentile of the pooled null distribution. Two-sample Kolmogorov–Smirnov tests (MATLAB `kstest2`, default alternative hypothesis) were performed to compare the pooled distributions.

Covariance maps (Fig. 2f) were produced by computing mean unmixed $\Delta F/F$ response during each stimulus presentation for each pixel, and computing the covariance between the two channels across stimulus presentations.

Multi-area imaging in mouse somatosensory cortex. In adult (6–8-week-old) C57Bl6 mice, stereotaxic viral injections of AAV2/9.*hSynapsin1*.jYCaMP1s were performed in to express jYCaMP in primary (S1) and secondary (S2) somatosensory cortex (600 nl total volume, 6.8×10^{11} gc ml^{-1}). L2/3 and L5 of S1 was targeted at 1.1 mm posterior to bregma, 3.3 mm lateral, 300 and 500 µm below the pial surface. L2/3 and L5 of S2 was targeted at 0.7 mm posterior to bregma, 4.2 lateral, 300 and 500 µm below the pial surface. Optical access over S1 and S2 was achieved by cranial window implantation. A metal headpost for head fixation was implanted on the skull surrounding the window. Imaging was performed with a custom-built resonant-scanning multi-area 2P microscope controlled by custom-written Scope software based on a design previously described[27]. The system consisted of a 31.25 MHz 1,040 nm ytterbium fiber laser (Spark Lasers) split into two temporally multiplexed beams positioned over S1 through a 1 × 6/0.8 NA water-immersion objective (Nikon). Simultaneous imaging was carried out at 32.6 Hz frame rate. All image processing was performed in MATLAB (Mathworks). The 2P images were motion corrected using a piece-wise rigid motion correction algorithm. Regions of interest corresponding to individual active neurons were manually identified and calcium signals computed as $(F - F_0)/F_0$ where F_0 represents the bottom eighth percentile of fluorescence across a 10 s sliding window.

***Drosophila* genetics.** We generated *w*^{1118}*;; PBac{20XUAS-IVS-GECI-p10}VK00005* transgenic lines carrying jYCaMP1. Sensors were driven in the Mi1 neurons using the *19F01-GAL4 (attp2)* and in Tm3 using the *59C10-GAL4 (attP2)* drivers. Males from sensor lines were crossed with females containing the driver lines. Flies were raised at 25 °C on standard cornmeal molasses media.

Imaging in *Drosophila* brain. Females 3–5 d after eclosure were anesthetized on ice. After transferring to a thermoelectric plate (4 °C), legs were removed, and then facing down, the head was glued into a custom-made pyramid using UV-cured glue. The proboscis was pressed in and fixed using UV-cured glue. After adding saline (103 mM NaCl, 3 mM KCl, 1 mM NaH_2PO_4, 5 mM TES, 26 mM $NaHCO_3$, 4 mM $MgCl^2$, 2.5 mM $CaCl_2$, 10 mM trehalose and 10 mM glucose, pH 7.4, 270–275 mOsm) to the posterior side of the head, cuticle was cut away above the right side creating a window above the target neurons. Tracheae and fat were removed. Muscles M1 and M6 were cut to minimize head movement.

The 2P imaging took place under a ×40 NA 0.8 water-immersion objective (Olympus) on a laser scanning microscope (BrukerNano) with GaAsP photomulitplier tubes. Laser power was kept constant at 8 mW using Pockel cells. No bleaching was evident at this laser intensity. The emission dichroic was 580 nm and emission filters 515/30–25 nm. Images were 128 × 128 pixels with a frame rate at 9.64 Hz.

A MATLAB script produced the visual stimulation via a digital micromirror device (LightCrafter) at 0.125 Hz onto a screen covering the visual field in front of the right eye. A blue led (474/23-25) emitting through a 474/23-25 bandpass filter provided illumination. At the fly's position, when 'ON', irradiance was measured at 2.5 mW m^{-2}.

Data analysis for *Drosophila* imaging. Using custom software written in python, regions of interest were segmented in the M8-10 medulla region for Mi1. When testing Tm3, columns were identified in the Lo1 region of the lobula plate. During testing, columns producing the maximum $\Delta F/F$ were identified by systematically testing layers until a maximum response was found. For each animal, the response over 2–3 columns was used to measure changes in fluorescence.

Statistics. Two-sided two-sample *t*-tests (MATLAB `ttest2`, default settings) were used to compare brightness and $\Delta F/F$ responses across indicators, with individual FOV as replicates (Figs. 1f,j,k and 2c,d and Supplementary Fig. 8b,d,g). Two-sample Kolmogorov–Smirnov tests (MATLAB `kstest2`, default settings) were performed to compare correlations between unmixed two-channel indicator responses to corresponding null distributions generated by bootstrapping, described above.

Reagent distribution. DNA constructs with jYCaMP1 variants are available at Addgene (plasmids 135420–135424; www.addgene.org/browse/article/28207200/). Fly lines are available through the Bloomington Drosophila Stock Center (stock no. 84970; https://bdsc.indiana.edu/). Sequences for jYCaMP and jYCaMP1s have been deposited in GenBank (MN808514; MN808515). Complete sequences for viral vectors are available from Addgene. Limited quantities of virus particles are available from the corresponding author.

Reporting Summary. Further information on research design is available in the Nature Research Reporting Summary linked to this article.

Data availability

Example raw datasets and summary statistics are available through Figshare; https://doi.org/10.25378/janelia.12098361. All other data associated with this study are available from the corresponding author.

Code availability

Custom code is available from the corresponding author, and at https://github.com/KasparP/twoColorUnmixing and github.com/KasparP/SLAP.

References

21. Studier, F. W. Stable expression clones and auto-induction for protein production in *E. coli*. *Methods Mol. Biol.* **1091**, 17–32 (2014).
22. Chen, T.-W. et al. Ultrasensitive fluorescent proteins for imaging neuronal activity. *Nature* **499**, 295–300 (2013).
23. Akerboom, J. et al. Genetically encoded calcium indicators for multi-color neural activity imaging and combination with optogenetics. *Front. Mol. Neurosci.* **6**, 2 (2013).
24. Akerboom, J. et al. Optimization of a GCaMP calcium indicator for neural activity imaging. *J. Neurosci.* **32**, 13819–13840 (2012).
25. Mütze, J. et al. Excitation spectra and brightness optimization of two-photon excited probes. *Biophys. J.* **102**, 934–944 (2012).
26. Wardill, T. J. et al. A neuron-based screening platform for optimizing genetically-encoded calcium indicators. *PLoS ONE* **8**, e77728 (2013).
27. Chen, J. L., Voigt, F. F., Javadzadeh, M., Krueppel, R. & Helmchen, F. Long-range population dynamics of anatomically defined neocortical networks. *Elife* **24**, e14679 (2016).

Acknowledgements

We thank H. Davies, C. Morkunas and M. Jeffries for logistical support and S. Di Lisio, K. Ritola, D. Walpita, J. Hasseman and the GENIE Project Team for experimental support. We thank S. Vishwanathan for the gift of Emx1-Cre mice. This work was funded by the Howard Hughes Medical Institute. M.A.M. was supported by the Janelia Graduate

Research Fellowship Program. E.J.M., C.-Y.L. and A.A. were supported by the Janelia Undergraduate Scholars Program. Work by J.L.C. and A.M.A. was supported by the National Science Foundation Neuronex Neurotechnology Hub (NEMONIC no. 1707287) and National Institutes of Health BRAIN Initiative Award (no. UF1NS107705).

Author contributions

K.P. conceived and K.P., E.R.S., J.S.M. and M.A.M. refined the idea. J.S.M. and M.A.M. produced Venus-GCaMPs. E.J.M. performed spectral screening with the help of K.P. C.-Y.L. M.A.M. and A.A. characterized proteins in vitro and M.A.M. and D.S.K. in cultured neurons. A.A. performed individual mutation depletion. Y.L. performed mouse virus injections. K.P., J.J.K. and M.A.M. performed mouse in vivo imaging. A.M.W. and M.A.M. generated fly lines and D.B. designed, performed and analyzed fly experiments. A.M.A. and J.L.C. designed and performed multi-area imaging experiments. R.P. and J.J.M. performed multiphoton spectroscopy and analyzed data. M.A.M., K.P., A.A., J.J.K., D.S.K. and E.R.S. analyzed data. M.A.M., K.P. and E.R.S. prepared the manuscript with input from all authors. K.P., E.R.S. and L.L.L. supervised the work.

Competing interests

The authors declare no competing interests.

Additional information

Supplementary information is available for this paper at https://doi.org/10.1038/s41592-020-0835-7.

Correspondence and requests for materials should be addressed to K.P.

Peer review information Rita Strack was the primary editor on this article and managed its editorial process and peer review in collaboration with the rest of the editorial team.

Reprints and permissions information is available at www.nature.com/reprints.

nature research

Corresponding author(s): Kaspar Podgorski

Last updated by author(s): Dec 11, 2019

Reporting Summary

Nature Research wishes to improve the reproducibility of the work that we publish. This form provides structure for consistency and transparency in reporting. For further information on Nature Research policies, see Authors & Referees and the Editorial Policy Checklist.

Statistics

For all statistical analyses, confirm that the following items are present in the figure legend, table legend, main text, or Methods section.

n/a	Confirmed
☐	☒ The exact sample size (*n*) for each experimental group/condition, given as a discrete number and unit of measurement
☐	☒ A statement on whether measurements were taken from distinct samples or whether the same sample was measured repeatedly
☐	☒ The statistical test(s) used AND whether they are one- or two-sided *Only common tests should be described solely by name; describe more complex techniques in the Methods section.*
☐	☒ A description of all covariates tested
☐	☒ A description of any assumptions or corrections, such as tests of normality and adjustment for multiple comparisons
☐	☒ A full description of the statistical parameters including central tendency (e.g. means) or other basic estimates (e.g. regression coefficient) AND variation (e.g. standard deviation) or associated estimates of uncertainty (e.g. confidence intervals)
☐	☒ For null hypothesis testing, the test statistic (e.g. *F*, *t*, *r*) with confidence intervals, effect sizes, degrees of freedom and *P* value noted *Give P values as exact values whenever suitable.*
☒	☐ For Bayesian analysis, information on the choice of priors and Markov chain Monte Carlo settings
☒	☐ For hierarchical and complex designs, identification of the appropriate level for tests and full reporting of outcomes
☐	☒ Estimates of effect sizes (e.g. Cohen's *d*, Pearson's *r*), indicating how they were calculated

Our web collection on statistics for biologists contains articles on many of the points above.

Software and code

Policy information about availability of computer code

Data collection	Microscopy data were collected using ScanImage 2017 software. Ratiometric screening was performed using custom Matlab-based software (R2017b, image acquisition toolbox),avaiilable from the corresponding author upon request. Neuron culture screens performed by the GENIE project used custom code described in Dana et al. 2019 (Nature Methods).
Data analysis	Fly data were analyzed using custom code written in Python 2. Mouse data were analyzed using custom code written in Matlab (R2017b onward), including the SLAP software package (github.com/KasparP/SLAP). Visual Stimuli were presented using Psychtoolbox 3 in Matlab. Structure visualization was produced with PyMol 2.2. Photophysical measurements were fit with custom Matlab software, Microsoft Excel 2013, and Prism 8 (Graphpad) software, as described in Methods. Custom code is available from the corresponding author upon request.

For manuscripts utilizing custom algorithms or software that are central to the research but not yet described in published literature, software must be made available to editors/reviewers. We strongly encourage code deposition in a community repository (e.g. GitHub). See the Nature Research guidelines for submitting code & software for further information.

Data

Policy information about availability of data

All manuscripts must include a data availability statement. This statement should provide the following information, where applicable:

- Accession codes, unique identifiers, or web links for publicly available datasets
- A list of figures that have associated raw data
- A description of any restrictions on data availability

Data are available from the corresponding author upon reasonable request.

Field-specific reporting

Please select the one below that is the best fit for your research. If you are not sure, read the appropriate sections before making your selection.

☒ Life sciences ☐ Behavioural & social sciences ☐ Ecological, evolutionary & environmental sciences

For a reference copy of the document with all sections, see nature.com/documents/nr-reporting-summary-flat.pdf

Life sciences study design

All studies must disclose on these points even when the disclosure is negative.

Sample size	For in vivo studies, we aimed to record from a predetermined 5 animals per condition, a common practice for preliminary studies in our field. Power analysis was not used to predetermine sample size.
Data exclusions	All completed experiments were included in analyses.
Replication	To our knowledge there have been no failed attempts to replicate these findings. We have distributed the indicators to several labs to aid in replication.
Randomization	For comparison of jGCaMP and jYCaMP, sex-matched littermates were injected with each of the two indicators on the same day and imaged in a single session for internal control. Apart from this, assignment to treatment groups was done without regard to any characteristics of individual subjects.
Blinding	Blinding was not performed. While technically possible, we did not attempt blinding due to the limited potential for bias in our assays, most of which are automated.

Reporting for specific materials, systems and methods

We require information from authors about some types of materials, experimental systems and methods used in many studies. Here, indicate whether each material, system or method listed is relevant to your study. If you are not sure if a list item applies to your research, read the appropriate section before selecting a response.

Materials & experimental systems

n/a	Involved in the study
☒	☐ Antibodies
☒	☐ Eukaryotic cell lines
☒	☐ Palaeontology
☐	☒ Animals and other organisms
☒	☐ Human research participants
☒	☐ Clinical data

Methods

n/a	Involved in the study
☒	☐ ChIP-seq
☒	☐ Flow cytometry
☒	☐ MRI-based neuroimaging

Animals and other organisms

Policy information about studies involving animals; ARRIVE guidelines recommended for reporting animal research

Laboratory animals	These studies involved live laboratory mice (Mus musculus, female, 6-8 weeks at study onset) and fruit flies (Drosophila melanogaster, 3-5 days after eclosure), as well as neonatal rat (Rattus norvegicus) hippocampal culture. Mouse strains used were C57B1/6J ('wild-type'), Emxl-Cre (B6.12952-Emxltml(cre)Krj/ J, Jackson Laboratories) and GP8.50 (Thyl::jRGECOla, provided by the GENIE project, HHMI Janelia Research Campus). We generated a transgenic jYCaMP reporter fly line (w1118;; PBac{20XUAS-IVS-GECI-pI0)VK00005), and use the (19F01-GAL4 (attp2)) and (59C10-GAL4 (attP2)) drivers.
Wild animals	The studies did not involve wild animals.
Field-collected samples	The studies did not involve field-collected samples.
Ethics oversight	Janelia Research Campus IACUC protocol # 17-155

Note that full information on the approval of the study protocol must also be provided in the manuscript.